

Nonmonotonic Stress Relaxation after Cessation of Steady Shear Flow  
in Supramolecular Assemblies

Peer-reviewed author version

Hendricks, Jan; Louhichi, Ameer; Metri, Vishal; Fournier, Remi; REDDY, Naveen;  
Bouteiller, Laurent; Cloitre, Michel; Clasen, Christian; Vlassopoulos, Dimitris & Briels,  
Wim (2019) Nonmonotonic Stress Relaxation after Cessation of Steady Shear Flow  
in Supramolecular Assemblies. In: Physical review letters (Print), 123 (21) (Art N° 218003).

DOI: 10.1103/PhysRevLett.123.218003

Handle: <http://hdl.handle.net/1942/30114>

# Non-monotonic stress relaxation after cessation of steady shear flow in supramolecular assemblies

Jan Hendricks,<sup>1,\*</sup> Ameer Louhichi,<sup>2,3,\*</sup> Vishal Metri,<sup>4</sup> Rémi Fournier,<sup>5</sup> Naveen Reddy,<sup>6</sup> Laurent Bouteiller,<sup>7</sup> Michel Cloitre,<sup>5</sup> Christian Clasen,<sup>1</sup> Dimitris Vlassopoulos,<sup>2,3,†</sup> and W.J. Briels<sup>4,8,‡</sup>

<sup>1</sup>*Department of Chemical Engineering, KU Leuven, 3001 Leuven, Belgium*

<sup>2</sup>*Institute of Electronic Structure & Laser, FORTH, P.O. Box 1527, 70013 Heraklion, Crete Greece*

<sup>3</sup>*Department of Materials Science & Technology,*

*University of Crete, Voutes Campus, 70013 Heraklion, Crete Greece*

<sup>4</sup>*Computational Chemical Physics, Faculty of Science and Technology,*

*and MESA+ Institute for Nanotechnology, University of Twente,*

*P.O. Box 217, 7500 AE, Enschede, The Netherlands*

<sup>5</sup>*Molecular, Macromolecular Chemistry, and Materials,*

*ESPCI Paris, CNRS, PSL University, 75005 Paris, France*

<sup>6</sup>*Faculty of Industrial Engineering, Hasselt University,*

*Martelarenlaan 42, 3500 Hasselt, Belgium, and IMO, IMOMECH,*

*Hasselt University, Wetenschapspark 1, 3590 Diepenbeek, Belgium*

<sup>7</sup>*Sorbonne Université, CNRS, IPCM, Equipe Chimie des Polymères, 75005 Paris, France*

<sup>8</sup>*ICS 3, Forschungszentrum Jülich, Wilhelm-Johnen-Straße, 52428 Jülich, Germany*

(Dated: September 29, 2019)

Stress relaxation upon cessation of shear flow is known to be described by single- or multi-mode monotonic exponential decays. This is considered to be ubiquitous in nature. However, we found that, in some cases, the relaxation becomes anomalous in that an increase in the relaxing stress is observed. Those observations were made for physico-chemically very different systems, having in common, however, the presence of self-associating units generating structures at large length scales. The non-monotonic stress relaxation can be described phenomenologically by a generic model based on an a redistribution of energy after the flow has stopped. When broken bonds are re-established after flow cessation, the released energy is partly used to locally increase the elastic energy by the formation of deformed domains. If shear has induced order such that these elastic domains are partly aligned, the re-establishing of bonds gives rise to an increase of the overall stress.

PACS numbers: 36.20.Fz, 83.50.Ha, 61.20.Qg, 81.16.Fg, 83.50.Ax, 83.10.-y, 83.85.St

Many experiments and simulations with soft materials ranging from polymer melts or solutions to colloidal suspensions, show that once an initially imposed shear rate is set to zero, the stress relaxes monotonically via one or more distinct exponential processes, reflecting successively the fast retraction of small-scale, shear-induced, non-equilibrium structures and the much slower relaxation of structures induced at the larger scales [1–5]. Often out-of-equilibrium systems such as colloidal glasses, pastes, and gels do not fully relax their stresses, but exhibit residual stresses because the induced large-scale structures cannot find relaxation pathways and remain permanent in the system [6–8]. Nonetheless, a common generic feature is the *monotonic* decrease of the stress to its final value. At first glance this appears to be the expected behavior, since no work that would be able to raise the stress is performed on the system. However, this scenario may not always hold. Indeed, for a particular supra-molecular polymer system, in which bonds were broken during steady shearing, we have found [9] a non-monotonic relaxation of stress following cessation of shear flow, as schematically shown in Fig. 1. In order to

prove the generic character of our findings, we have investigated two more, physically and chemically very different systems, with different associating mechanisms [10, 11]. All cases have in common that bonds are disrupted by subjecting the systems to steady shear flow, and reform after flow cessation. We argue below that a redistribution of the released bond-energy during stress relaxation gives rise to a temporary stress increase. Hence, the purpose of this letter is to present and rationalize this counter-intuitive non-monotonic stress relaxation upon cessation of steady shear flow. Non-monotonic stress evolution has, of course, been observed in driven systems, during start-up with stress overshoots, and in banding systems where even stress undershoots may occur during the development of the bands [12–14].

The first system (A) examined is an organogel consisting of 2,4-bis (2-ethyl-hexyl-ureido) toluene (EHUT) [15, 16] dissolved in dodecane, an apolar solvent. The EHUT bis-urea based monomers self-assemble above a certain concentration, through the formation of hydrogen bonds between the urea groups. Data presented in this paper was obtained in the tube region of the phase diagram (with cross-sectional diameter of three EHUT monomers or  $\sim 2.6$  nm) [17] at a concentration of  $12 \text{ g L}^{-1}$ , where the tubes are long enough to entangle and exhibit a rich viscoelastic response.

The second system (B) comprises aqueous solutions of

\* These two authors contributed equally

† Dimitris Vlassopoulos: [dvlasso@iesl.forth.gr](mailto:dvlasso@iesl.forth.gr)

‡ W.J. Briels: [W.J.Briels@utwente.nl](mailto:W.J.Briels@utwente.nl)

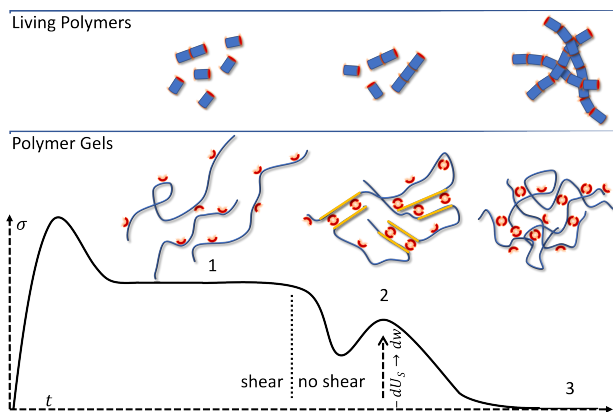


FIG. 1. (Color online) Illustration of the experimental protocol and structural changes of the investigated living polymers (system A) and polymer gels (systems B and C) under shear and during relaxation. Large shear magnitudes lead to bond breakage resulting in stored energy (1). Bond reformation leads to work performed on the polymers and causes local elastic inhomogeneities, indicated by orientationally correlated local segments marked by yellow lines, resulting in increasing bulk stress (2), which eventually relaxes thermally until the equilibrated networks of living polymers or polymer gels are re-established (3).

a synthetic polymer having a molar mass of  $500 \text{ kg mol}^{-1}$ , with 5% of the monomers being functionalised with ligands [18]. Polymer solutions with concentrations corresponding to the semi-dilute regime (1.35 wt%) were mixed with a stoichiometric concentration of metal ions to ligands. The added iron chloride results in strong metal-ligand bonded supra-molecular hydrogels, with up to three ligands bonded to a single metal ion.

The third system (C) consists of two complementary polymers dissolved at low concentrations (0.35 wt% each) in 0.1 M aqueous NaOH at pH=12.5. [11]. The first polymer is a partially hydrolysed polyacrylamide grafted with phenylboronic acid moieties (HPAM-g-PBA) with a molar mass of  $780 \text{ kg mol}^{-1}$ , and the second polymer is a fully saponified poly(vinylalcohol) (PVA) with a molar mass of  $125 \text{ kg mol}^{-1}$ . The phenylboronic acid moieties and the 1,3 diols form phenylboronic esters. Reversible covalent bonds are formed. Despite their low equilibrium constants ( $K < 10 \text{ L mol}^{-1}$ ), gels in the semi-dilute unentangled regime are formed at polymer concentrations below 2 wt%, due to synergistic effects of multiple associations.

Details about rheological measurements are found in the Supplemental Material (SM). Fig. S1 of the SM presents the linear viscoelastic spectra of the three systems. The range of shear rates applied before flow cessation corresponds to the frequency region associated with the breaking time of associations (above the minimum in  $G''$ ) and justifies the induced orientation at steady state (Fig. 1).

Experimental stress relaxation curves after flow cessation are shown in Fig. 2 for all three systems and for

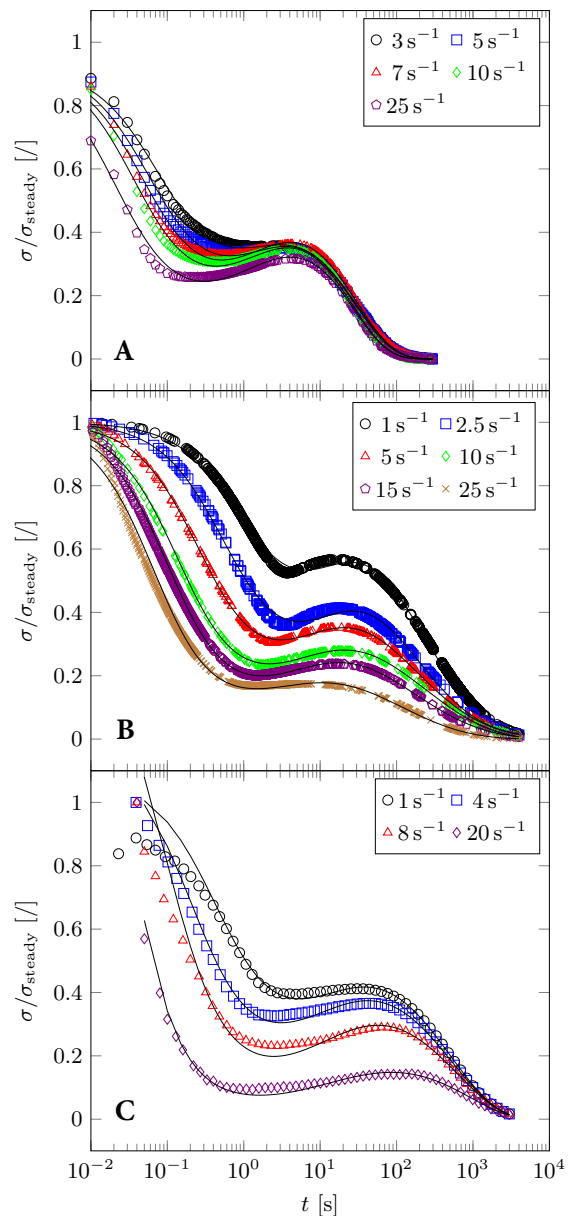


FIG. 2. (Color online) Stress relaxation experiments with the supramolecular systems A (top), B (middle), and C (bottom). At intermediate times stresses increase. The shear stress is normalized to the steady state shear stress, and shear rates applied prior to cessation of flow are listed in the legends.

different initially imposed shear rates. Time zero was set when the steady shear flow was stopped, and stresses have been normalized by their values at time zero. In all cases the stress relaxation is clearly non-monotonic. Stresses in system A have already decayed substantially at the earliest times shown in the plot. This is because early relaxation of small species (see also cartoon illustration in Fig. 2) is too fast to be resolved [9]. We note that all stresses relax eventually to zero at times of the

order of the terminal time of the linear stress relaxation modulus  $G(t)$ , which is the Fourier transformation of  $G'$  and  $G''$  [19].

Repeat runs of all experiments with newly prepared batches of the various systems confirmed our findings. Additional support from birefringence measurements and an analysis of possible motor drift (see SM) confirm that the effect, although unexpected, is real. The fact that birefringence follows the stress upswing (Fig. S3) implies local orientation (see also Fig. 1). The main reason for not expecting an upswing of an initially decaying stress is the possible disagreement with either of the two laws of thermodynamics. We will now argue that this is not the case and suggest a very simple, highly approximate phenomenological model to describe our data.

In general, the microscopic state of the system is described by local strains, local order tensors, and local bond densities. The steady-state values of strain rate  $\dot{\gamma}$  and total strain  $\gamma$  fix the initial values for these variables. A set of evolution equations then allows the calculation of these variables at later times. The evolution equations should naturally contain random contributions obeying appropriate fluctuation-dissipation theorems. Here, we restrict ourselves to the more modest task of describing only the stress relaxation after the shear has stopped, thereby eliminating the need to include random contributions to the evolution equations. We assume that local strains and local order basically describe the same aspect of our systems, and focus on strains. Since stress is an increasing function of strain we replace stresses by strains in the list of state variables. Although much of our argumentation is about local stresses, our final model uses only global properties of the system.

Our considerations suggest the following set of evolution equations

$$df = -rfdt, \quad (1)$$

$$d\sigma_{xy} = -\sigma_{xy}\frac{dt}{\tau} - \sigma_{xy}Bdf. \quad (2)$$

Here  $f$  is the fraction of all bonds that are broken, and  $\sigma_{xy}$  is the measured shear stress. The coordinate frame is such that the imposed steady shear flow was in the x-direction with its gradient in the y-direction. Both  $f$  and  $\sigma_{xy}$  depend explicitly on time with increments  $df$  and  $d\sigma_{xy}$  during a time interval  $dt$ . The parameters  $r$ ,  $\tau$  and  $B$  depend implicitly on time through their dependence on  $f$ . The first equation tells us that the fraction of broken bonds decays with rate  $r$ . The second equation indicates that the stress decays at a time scale  $\tau$  due to erratic motions in the system, while it increases when bonds are re-established; with  $df$  being negative, the effective bond contribution to the stress  $B$  must be positive in order to describe stress increase.

We consider the system to be isolated immediately after shearing has been stopped and describe how energy is redistributed while bonds are re-established and the system relaxes to equilibrium. The bond energy density  $U_B$  at any instant of time may be written as  $U_B = (1 - f)\Phi$  with  $f$  being time dependent. At equilibrium,  $f = 0$  and

the bond energy density equals  $\Phi$ . Notice that with this definition  $\Phi$  is negative, and that by breaking bonds an energy density of  $U_S = -f\Phi$  has been stored into the system. The total energy density  $U_{\text{tot}}$  reads

$$U_{\text{tot}} = U_T + U_E + U_B, \quad (3)$$

where  $U_T$  is the thermal energy density, *i.e.* the part of the energy density that depends only on temperature, and  $U_E$  the elastic energy density, *i.e.* the part of the energy density that depends both on temperature and on (local) strain. Since we are considering an isolated system, the total energy density will remain constant during the relaxation process, while the individual contributions depend on time.

During the approach to equilibrium after cessation of flow, the fraction of broken bonds gradually decreases from its initial value  $f_0$  to zero at long times, while concomitantly the stored energy decreases to zero. We assume that the released binding energy will be partly delivered as thermal energy, and partly as elastic energy. During a small time interval, therefore, we may write

$$\begin{aligned} dU_B &= -\Phi df \\ dU_T &= dU_{\text{err}} + (1 - \alpha)\Phi df \\ dU_E &= -dU_{\text{err}} + \alpha\Phi df, \end{aligned} \quad (4)$$

where  $\alpha$  denotes the fraction of binding energy released as elastic energy.  $dU_{\text{err}}$  is the amount by which the elastic energy decays due to erratic motions of prevailing non-equilibrium associated polymer structures, living polymers in the case of the EHUT system. This is the process that gives rise to the first term in the right hand side of Eq. 2. The released energy due to bond formation,  $dU_S = -dU_B = \Phi df$ , has been split into a part  $(1 - \alpha)\Phi df$  delivered as heat and a part  $\alpha\Phi df$  delivered as work done on the elastic component of the energy. Notice that when bonds are formed,  $df$  is negative and  $\Phi df$  is positive. Clearly, we do not know how much of the released energy  $\Phi df$  is delivered as work, and how much as heat. The second law of thermodynamics requires  $(1 - \alpha)\Phi df$  to be large enough so that the corresponding increase of entropy outweighs the decrease of entropy resulting from the change of elastic energy (through a change of local strains). Within these limits, the elastic energy will increase by an amount  $\alpha\Phi df$ . Near equilibrium, the second law of thermodynamics states that stress increases monotonically with increasing elastic energy. Since torque measurements with a rheometer are instantaneous, we conclude that the stress increases proportionally to  $-df$ . In order to comply with the tensor character of the stress, the constant of proportionality has to transform as a tensor. The only tensor we can use is stress itself, leading to the contribution  $-\sigma_{xy}Bdf$  in Eq. 2.

Notice that  $B$  accounts for the combined effect of two different aspects of the relaxation process. First, we have assumed that bond formation can lead to work being done on the surroundings of two associating structural elements. Second, we have attributed a measurable shear

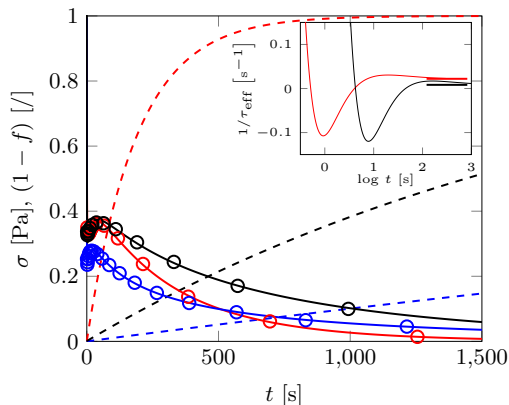


FIG. 3. (Color online) Increase of fraction of formed bonds following flow cessation,  $1 - f$ , with time along with the stress evolution for systems A, B and C, respectively, in red, blue, and black at initial shear rates of  $7 \text{ s}^{-1}$ ,  $10 \text{ s}^{-1}$  and  $4 \text{ s}^{-1}$ . The circles are experimental stress data, lines are the model fits and dashed lines are the associated  $1 - f$  values. For system A in red, the time axis has been multiplied by 10 so that all data fit into the same plot. Inset: Variation of the inverse effective stress decay time  $(\tau_{\text{eff}})^{-1}$  with time (see text). Horizontal lines indicate the inverse decay times  $1/\tau_l$  to be reached at very long times.

stress increase to the locally increased elastic energy. In many situations this is actually not the case. Suppose that the bonding process leads to a system containing many randomly oriented elastically deformed domains. All off-diagonal components of the stress tensor will then on average be zero, much like the overall magnetization of a collection of magnetized Weiss domains is zero when they are randomly oriented. So, a basic assumption underlying our equations is that the induced elastic domains are not isotropically oriented, but rather have an average orientation that gives rise to a non zero contribution to the  $xy$ -component of the stress tensor.

In order to complete the model, we need constitutive equations for  $r$ ,  $\tau$  and  $B$  in terms of  $f$ . For simplicity, and in order to limit the number of unknown parameters, we make the following choice:

$$\begin{aligned} r(f) &= r \\ \tau(f) &= \tau_l - (\tau_l - \tau_s) \frac{f}{f_0} \\ B(f) &= b(1 - f)^{-\kappa}. \end{aligned} \quad (5)$$

The first assumes that the relative rate with which new bonds are created is constant. Depending on the type of reaction, one might consider other forms here. The second is a simple linear interpolation in  $f$  of the instantaneous relaxation time  $\tau_s$  and a long time relaxation time  $\tau_l$ . The reasoning behind the third expression is that what really matters for stress increase is the relative increase of the fraction of bonds materialized; in order to be more flexible we have changed the dependence on  $(1 - f)^{-1}$  into  $(1 - f)^{-\kappa}$ , with  $\kappa$  being a constant.

With this model we have fitted the experimental findings and plotted the results as drawn lines in Fig. 2. First of all, it is clear that the model, given its simplicity, captures the experimental data very well, with the only noticeable disagreement being near the stress minima. It is reassuring to notice that in all cases the position of the maxima are well described.

The main reason why the model is able to describe the data is the fact that the stress evolving with time is the sum of two competing terms, where the first leads to a stress decrease while the second may lead to a stress increase depending on the sign of  $B$ . We have argued above that, depending on the interplay between shear induced order and bond formation, stress increase may be expected. The absolute values of both terms are decreasing with time, which does not imply, however, that they may never become equal. In order to clarify this point we combine Eqs 1 and 2 to find  $d\sigma_{xy} = -\sigma_{xy}dt/\tau_{\text{eff}}$ , where  $\tau_{\text{eff}}$  is an effective decay time given by

$$\frac{1}{\tau_{\text{eff}}} = \frac{1}{\tau}(1 - Brf\tau). \quad (6)$$

In the inset of Fig. 3 we have plotted  $1/\tau_{\text{eff}}$  as a function of time for systems A and C. Initially and at late times  $\tau_{\text{eff}}$  is positive, giving rise to decaying stresses. At intermediate times  $\tau_{\text{eff}}$  is negative, causing the stress to increase. At these times  $Brf\tau$  is larger than one, implying that the natural stress decay cannot compete with the stress increase due to the formation of new bonds. Thus, stresses are increasing. When  $t$  goes to infinity,  $f$  goes to zero and therefore both  $\tau$  and  $\tau_{\text{eff}}$  go to  $\tau_l$ . The values of  $1/\tau_l$ , obtained from the fits, are indicated as short drawn lines to the right of the inset in Fig. 3. It is interesting that the stress of the first system (A) decays exponentially in time soon after having reached its maximum, reflecting the Maxwellian relaxation of living polymers. The same does not apply in the other two cases, where the increase of the fraction of bonds is much slower. The stress decay after the maximum is described by a stretched exponential with exponents 0.54 for system B, and 0.85 for system C. In Fig. 3 we plot the time dependence of both the stress and the fraction of bonds materialized in the system,  $1 - f(t)$ . Note that the horizontal axis indicates seconds for systems B and C, and tens of seconds for system A. As an aside, let us mention that the EHUT system stops showing a stress increase when the steady shear flow is prolonged to very high strain values. In this case the initially broken polymers start to reform during the shearing stage in a shear aligned state. After cessation of flow no new bonds are being created, and the system simply decays exponentially as a living polymer.

In all cases  $\kappa$  was only slightly above one, while the initial value  $f_0$  was only slightly below one. For the EHUT system this is not surprising. For the polymer systems this implies that the model in its present form is slightly oversimplified. In these cases, steady shearing has two effects. First it will disrupt bonds leading to a decay of the bond density, as included in our model.  $f = 1$  does

not refer to all bonds being broken, but to a the maximum of bonds that can be broken by shearing the system. Second, depending on the total strain, it shifts the distribution of the remaining bonds over intramolecular and intermolecular bonds away from the corresponding equilibrium distribution. After all broken bonds have been re-established, during the later part of the stress relaxation, the disturbed distribution of bonds must re-equilibrate. This needs existing bonds to be broken and re-establish elsewhere. The time-scale for this process must be set by an activation barrier of the order of the binding energy. This is only implicitly described in the present model.

The ingredients that a system must have in order to exhibit non-monotonic stress relaxation after cessation of flow, are twofold. First, the system should contain functional groups that are able to form bonds. The strength of the bonds must be such that the system accumulated elastic energy. Second, bond formation should be able to locally deform the material and induce stress. For the associative polymers this sets an upper limit to the bond densities. On the other hand, possible binding partners must meet before the order imposed by the shear has relaxed completely. In order to generate macroscopically measurable stresses, the stresses induced by the forma-

tion of bonds at different positions in the system must at least partly be aligned, as confirmed by the increase of birefringence (Fig. S3).

In summary, we have provided experimental evidence for the unexpected non-monotonic stress relaxation upon cessation of shear flow in different associating systems. Our novel findings are rationalized by a simple phenomenological model which ensures thermodynamic consistency and bear strong similarities to the polymerisation of microtubules [24, 25] (in particular with system A), which possess force generating mechanisms by performing work with energy provided by adenosine triphosphate (ATP) or guanosine triphosphate (GTP) [26], e.g. power strokes and ratchets [27], can heal defects [28], and are flow sensitive [29]. This sets the framework for further exploring and understanding of the physics of relaxation phenomena in synthetic and biological systems and paves the way for detailed structural experiments or simulations to exploit the possible anisotropic orientation of induced elastic domains.

#### ACKNOWLEDGMENTS

We acknowledge support by the EU (FP7, Marie-Curie ITN, grant no. 607937-SUPOLEN).

- 
- [1] Y. Serero, V. Jacobsen, J. F. Berret, and R. May, *Macromolecules* **33**, 1841 (2000).
  - [2] L. Pellens, R. Gamez Corrales, and J. Mewis, *Journal of Rheology* **48**, 379 (2004).
  - [3] S. Suzuki, T. Uneyama, T. Inoue, and H. Watanabe, *Macromolecules* **45**, 888 (2012).
  - [4] F. Meng, R. H. Pritchard, and E. M. Terentjev, *Macromolecules* **49**, 2843 (2016).
  - [5] M. K. Sing, J. Ramirez, and B. D. Olsen, *J. Chem. Phys.* **147** (2017).
  - [6] M. Ballauff, J. M. Brader, S. U. Egelhaaf, M. Fuchs, J. Horbach, N. Koumakis, M. Krüger, M. Laurati, K. J. Mutch, G. Petekidis, M. Siebenbürger, T. Voigtmann, and J. Zausch, *Phys. Rev. Lett.* **110**, 215701 (2013).
  - [7] E. Moghimi, A. R. Jacob, and G. Petekidis, *Soft Matter* **13**, 7824 (2017).
  - [8] L. Mohan, R. T. Bonnecaze, and M. Cloitre, *Phys. Rev. Lett.* **111** (2013).
  - [9] A. Louhichi, *Supramolecular assemblies and networks: interactions, viscoelasticity and flow*, Ph.D. thesis, Univ. of Crete (2017).
  - [10] J. Hendricks, *Supramolecular Polymeric Solutions in Shear and Extensional Flows (in preparation)*, Ph.D. thesis, KU Leuven (2019).
  - [11] R. Fournier, *Polymères associatifs par interaction covolente réversible diol-acide boronique*, Ph.D. thesis, Univ. Pierre et Marie Curie (Paris) (2016).
  - [12] J. K. G. Dhont, *Phys. Rev. E* **60**, 4534 (1999).
  - [13] C. Pujolle-Robic, P. D. Olmsted, and L. Noirez, *Europhys. Lett.* **59**, 364 (2002).
  - [14] J. Mewis and P. Moldenaers, *Mol Cryst Liq Cryst* **153**, 291 (1987).
  - [15] G. Ducouret, C. Chassenieux, S. Martins, F. Lequeux, and L. Bouteiller, *J. Colloid Interface Sci.* **310**, 624 (2007).
  - [16] T. Shikata, T. Nishida, B. Isare, M. Linares, R. Lazzaroni, and L. Bouteiller, *J. Phys. Chem. B* **112**, 8459 (2008).
  - [17] L. Bouteiller, O. Colombani, F. Lortie, and P. Terech, *J. Am. Chem. Soc.* **127**, 8893 (2005).
  - [18] J. Brassinne, A. Cadix, J. Wilson, and E. van Ruymbeke, *J. Rheol.* **61**, 1123 (2017).
  - [19] See Fig. S2 and relevant discussion in the supplementary material, which includes Refs. [20-23].
  - [20] A. Louhichi, A. R. Jacob, L. Bouteiller, and D. Vlasopoulos, *J. Rheol.* **61**, 1173 (2017).
  - [21] M. Akbulut, N. K. Reddy, B. Bechtloff, S. Koltzenburg, J. Vermant, and R. K. Prud'homme, *Langmuir* **24**, 9636 (2008).
  - [22] G. G. Fuller, *Optical rheometry of complex fluids* (Oxford University Press on Demand, 1995).
  - [23] L. Pellens, J. Vermant, and J. Mewis, *Macromolecules* **38**, 1911 (2005).
  - [24] A. Desai and T. J. Mitchison, *Annu. Rev. Cell Dev. Biol.* **13**, 83 (1997).
  - [25] C. P. Brangwynne, F. C. MacKintosh, and D. A. Weitz, *Proc. Natl. Acad. Sci. U. S. A.* **104**, 16128 (2007).
  - [26] S. Inoue and E. D. Salmon, *Mol. Biol. Cell* **6**, 1619 (1995).
  - [27] A. Mogilner and G. Oster, *Curr. Biol.* **13**, R721 (2003).
  - [28] L. Schaedel, K. John, J. Gaillard, M. V. Nachury, L. Blanchoin, and M. Thery, *Nat. Mater.* **14**, 1156 (2015).
  - [29] K. Okeyoshi, R. Kawamura, R. Yoshida, and Y. Osada, *Sci Rep* **5** (2015).

# Supplemental Material: Non-monotonic stress relaxation after cessation of steady shear flow in supra-molecular assemblies

Jan Hendricks,<sup>1,\*</sup> Ameer Louhichi,<sup>2,3,\*</sup> Vishal Metri,<sup>4</sup> Rémi Fournier,<sup>5</sup> Naveen Reddy,<sup>6</sup> Laurent Bouteiller,<sup>7</sup> Michel Cloitre,<sup>5</sup> Christian Clasen,<sup>1</sup> Dimitris Vlassopoulos,<sup>2,3,†</sup> and W.J. Briels<sup>4,8,‡</sup>

<sup>1</sup>*Department of Chemical Engineering, KU Leuven, 3001 Leuven, Belgium*

<sup>2</sup>*Institute of Electronic Structure & Laser, FORTH, P.O. Box 1527, 70013 Heraklion, Crete Greece*

<sup>3</sup>*Department of Materials Science & Technology,*

*University of Crete, Voutes Campus, 70013 Heraklion, Crete Greece*

<sup>4</sup>*Computational Chemical Physics, Faculty of Science and Technology,*

*and MESA+ Institute for Nanotechnology, University of Twente,*

*P.O. Box 217, 7500 AE, Enschede, The Netherlands*

<sup>5</sup>*Molecular, Macromolecular Chemistry, and Materials,*

*ESPCI Paris, CNRS, PSL University, 75005 Paris, France*

<sup>6</sup>*Faculty of Industrial Engineering, Hasselt University,*

*Martelarenlaan 42, 3500 Hasselt, Belgium, and IMO, IMOMECH,*

*Hasselt University, Wetenschapspark 1, 3590 Diepenbeek, Belgium*

<sup>7</sup>*Sorbonne Université, CNRS, IPCM, Equipe Chimie des Polymères, 75005 Paris, France*

<sup>8</sup>*ICS 3, Forschungszentrum Jülich, Wilhelm-Johnen-Straße, 52428 Jülich, Germany*

## I. RHEOLOGICAL MEASUREMENTS

The response to shear in the first system was measured immediately after preparation with a strain-controlled ARES rheometer (TA Instruments, USA) equipped with a stainless steel cone-and-plate geometry of 25 mm radius and 0.04 rad cone angle, at a temperature of 20 °C. Given the great sensitivity of the self-assembly to humidity because of competing hydrogen-bonding interactions, measurements were carried out in dry conditions using a homemade drying chamber described by Louhichi et al. [20]. Measurements on the second system were performed at room temperature in a double-wall Couette geometry on an ARES-G2 rheometer (TA Instruments, USA). Data for the third system were obtained at room temperature with a MCR 502 stress-controlled rheometer operating in strain-controlled mode (Anton-Paar, Austria) using a stainless steel cone and plate geometry of 25 mm radius and a mineral oil immersion to reduce evaporation. A steady state of partially broken bond structures was assured for the hydrogels by subjecting them to constant shear rates for a fixed time, between 2000 s and 4000 s, while the EHUT solution was submitted to a fixed deformation of 25 strain units. In all cases temperature was controlled to about  $\pm 0.1$  K by means of Peltier elements.

The linear viscoelastic spectra of systems A, B, and C used in relaxation experiments are shown in Fig. S1. They are served to provide a means of characterization of the linear viscoelasticity of the systems, showing qualitative and quantitative differences. For example, in system A one may distinguish the high-frequency peak in  $G''$ , which is associated with the breaking time, as well as the relatively high value of the plateau modulus [20]. The

gray areas indicate the regimes of linear response which correspond to the range of shear rates applied in the experiments processing the relaxation upon flow cessation (all well above the terminal frequency, in the neighborhood of the  $G''$  minimum).

The shear modulus is compared in Fig. S2 with the stress relaxation data of Fig. 2, although due to limited linear data at long times, the interpretation is to some degree speculative. The overall relaxation behavior is related but differences are observed at long times. No definite conclusion can be drawn by comparing the linear response with the slow relaxation mode following cessation of shear flow, but it is evident that the two are related, i.e., the slow relaxation somehow follows the linear  $G(t)$ . This is expected in general for systems that equilibrate reasonably fast, like entangled polymers. On the other hand, the differences which are particularly evident in systems B and C, might originate from the fact that before flow cessation the systems are out of equilibrium, hence the subsequent stress relaxation measurements differ from the  $G(t)$  ones.

## II. RHEO-OPTICAL MEASUREMENTS

Rheo-optical measurements were performed complementary to the stress relaxation experiments presented in the main paper. Polarimetry techniques can provide additional insight into a fluids microstructure and reveal e.g. flow induced conformational changes of polymers, when combined with a rheometer [21]. Generally, polarimetry describes the alteration of light polarization by an anisotropic material structure that reflects in refractive index differences [22]. Exposing a sample to shear can induce anisotropy due to orientation and stretching of the fluids micro-structure and consequently alter the refractive index,  $n = n' - in''$ . The real part is related to an orientation dependent retardation  $\delta'$  of transmitted light, and therefore a phase shift between incoming and

\* These two authors contributed equally

† Dimitris Vlassopoulos: [dvlasso@iesl.forth.gr](mailto:dvlasso@iesl.forth.gr)

‡ W.J. Briels: [W.J.Briels@utwente.nl](mailto:W.J.Briels@utwente.nl)

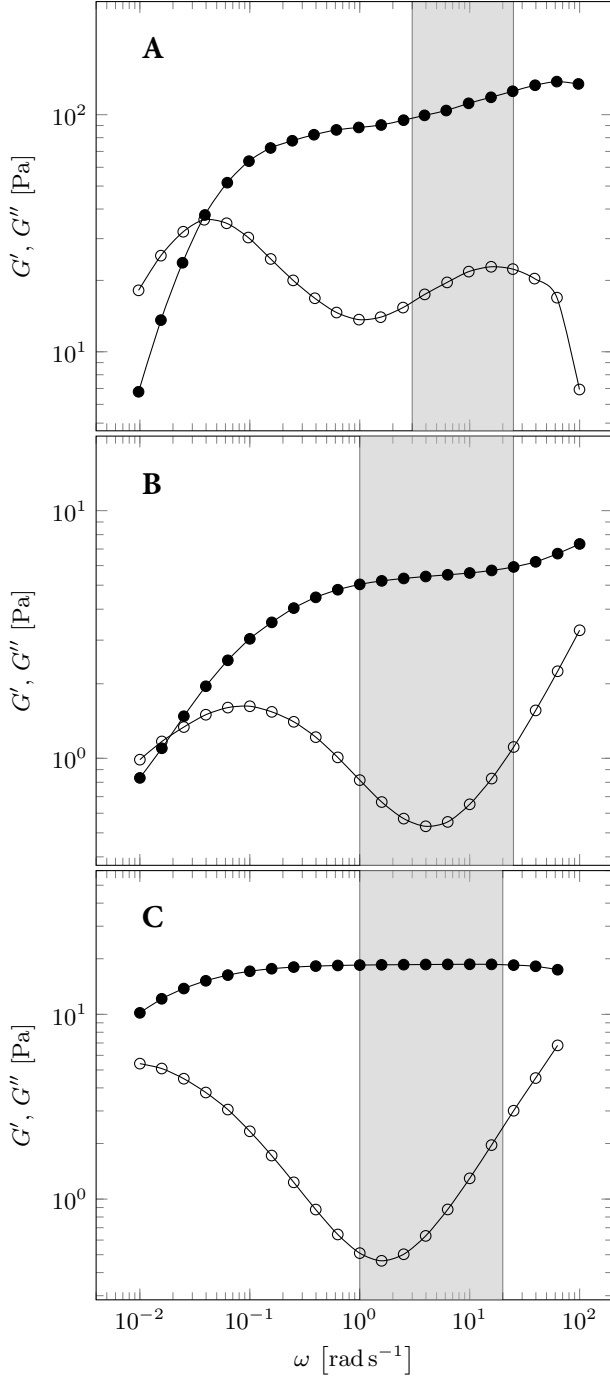


FIG. S1. Frequency-dependent storage ( $G'$ , filled symbols) and loss ( $G''$ , open symbols) moduli of systems A (top), B (middle), and C (bottom).

outgoing light, whereas the complex part causes an attenuation  $\delta''$  of the light. Birefringence is the difference of the real part of the refractive index in two principle

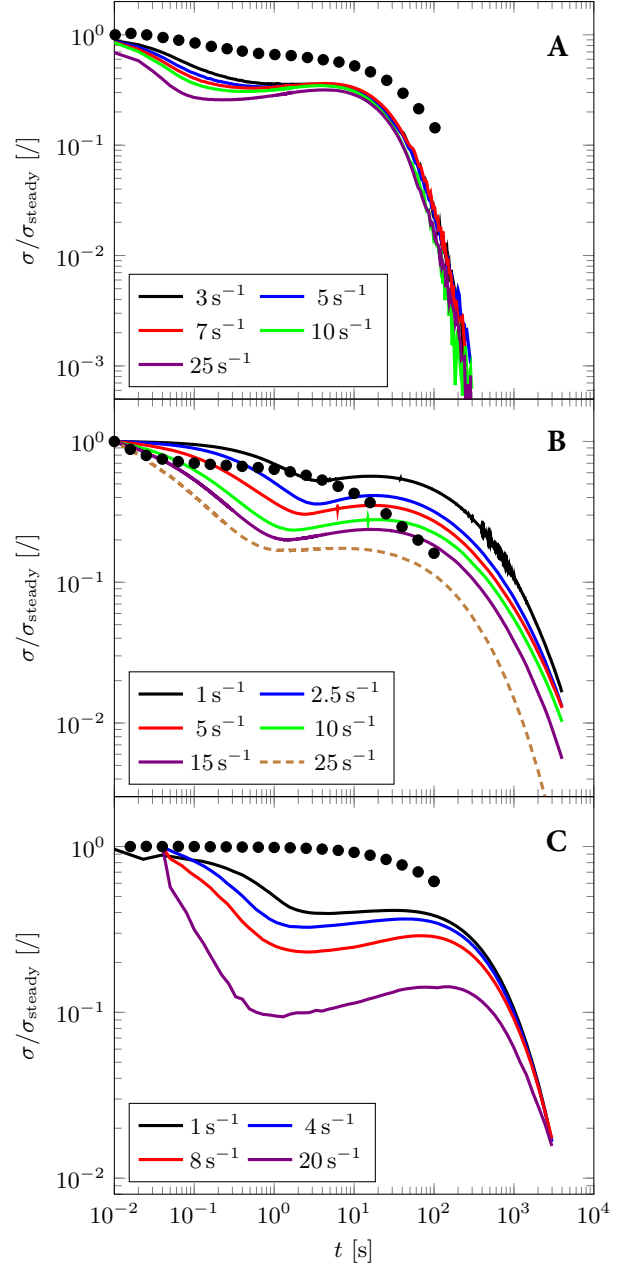


FIG. S2. (Color online) Experimental stress relaxation data as presented in Fig. 2 (lines) compared to the normalized magnitude of the shear modulus,  $|G^*|(t = 1/\omega)$ , obtained from the linear data shown in Fig. S1 (dots).

directions and is related to this retardation as

$$\Delta n' = \frac{\lambda \delta'}{2\pi d} \quad , \quad (1)$$

with  $\lambda$  as the wavelength of the light and  $d$  the path length through the sample. Birefringence can thus be used as a stress independent measure to probe the evolution of structural anisotropy within the area of interest in the current paper, the non-monotonic stress relaxation,

and is particular in the region of stress upswing.

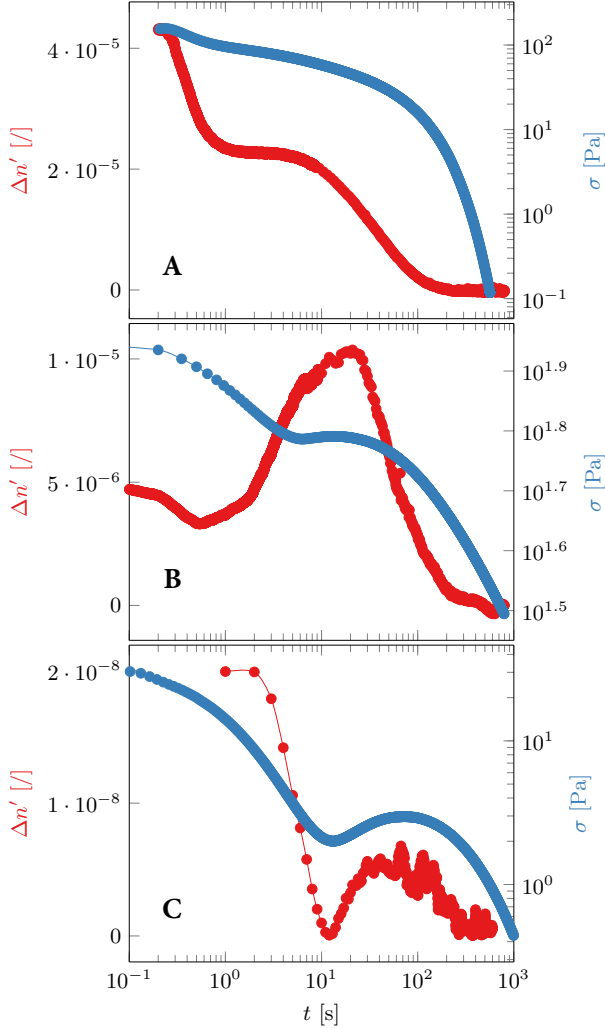


FIG. S3. (Color online) Evolution of shear stress,  $\sigma$ , after cessation of steady shear along with the recorded birefringence signal,  $\Delta n'$ , (top) system A sheared at 20 1/s for 1 s, (middle) system B sheared at 1 1/s for 60 s, and (bottom) system C sheared at 5 1/s for 120 s. The investigated sample compositions differ slightly from the compositions investigated in Fig. 2, resulting in deviations of the stress increase.

Rheo-Optical measurements were done with a home-built device based on an MCR-300 stress controlled rheometer (Anton Paar, Austria) combined with an optical pathway to measure linear flow birefringence based on photoelastic modulation [23]. Two rheometrical glass geometries were used: a plate-plate geometry with a diameter of 43 mm for the first and third system and a Couette geometry of 16.4 mm height and inner and outer radii of, respectively, 16.0 mm and 18.0 mm, for system B. Sample A and C were measured using a plate-plate geometry as they are highly viscous making it difficult to load into the Couette cell and easily fractured under shear. Consequently, the velocity/velocity gradient

plane is probed using a Couette geometry, whereas the velocity/vorticity plane is probed in a plate-plate geometry. The measurement gap for the plate-plate geometry was chosen to maximize the birefringence signal intensity and is in the range between 1 mm and 3 mm. All experiments were performed at room temperature (22 °C). Light is generated by a He-Ne laser with a wavelength of  $\lambda = 632$  nm which is sent through a Glan-Thompson polarizer at  $0^\circ$ , followed by a feedback-stabilized photoelastic modulator (Beaglehole Instruments, New Zealand) and a quarter wave plate at  $0^\circ$ . The photoelastic modulator consists of a piezoelectric transducer coupled with fused silica and has a resonance frequency at 50 kHz, leading to a variable retardance (birefringence) of

$$\delta'_{\text{PEM}} = A \sin(\Omega t) \quad (2)$$

with the amplitude  $A$  controlled by the gauge voltage and  $\Omega = 50$  kHz as the resonance frequency. After the light beam passes the sample, it is passed through an analyzer consisting of a quarter wave plate at  $45^\circ$  and a Glan-Thompson polarizer at  $0^\circ$ . Finally, the light intensity is measured by a photo diode (Beaglehole Instruments, New Zealand). The DC is recorded with a data acquisition card. SR830 lock-in amplifiers (Stanford Research Systems, USA) were used to determine the first and second harmonic signals with the 50 Hz signal generated by the photoelastic modulator as reference. For a purely birefringent sample with zero extinction ( $\delta'' = 0$ ), the light intensity is given by

$$I = \frac{I_0}{4} (1 - (J_0(A) + 2J_2(A) \cos \Omega t) \sin 2\chi \sin \delta' + (2J_1(A) \sin \Omega t) \cos 2\chi \sin \delta') \quad (3)$$

with  $J_m$  as Bessel functions of  $m$ th order,  $I_0$  the intensity of the laser beam,  $\delta'$  the phase difference between the fast and slow axis (retardation) and  $\chi$  the orientation angle of the birefringence with respect to the flow direction. The gauge voltage of the photoelastic modulator is set such that  $J_0(A) = 0$ . The DC signal

$$I_{\text{DC}} = \frac{I_0}{2} \quad (4)$$

and the first and second harmonics, respectively,  $I_\Omega$  and  $I_{2\Omega}$ , obtained from the AC signal and normalized by the DC signal are

$$\begin{aligned} \frac{I_\Omega}{I_{\text{DC}}} &= 2J_1(A) \cos 2\chi \sin \delta' \\ \frac{I_{2\Omega}}{I_{\text{DC}}} &= -2J_2(A) \sin 2\chi \sin \delta' \end{aligned} \quad (5)$$

to determine the birefringence

$$\Delta n' = \frac{\lambda \delta'}{2\pi d} \quad (6)$$

with the sample thickness  $d$ , the retardation

$$\delta' = \arcsin \left( \frac{1}{2} \sqrt{\left( \frac{I_{\Omega}}{J_1(A)I_{DC}} \right)^2 + \left( \frac{I_{2\Omega}}{J_2(A)I_{DC}} \right)^2} \right) \quad (7)$$

and the orientation angle

$$\chi = \frac{1}{2} \arctan \left( -\frac{J_1(A)I_{2\Omega}}{J_2(A)I_{\Omega}} \right). \quad (8)$$

Birefringence was set to zero before starting an experiment corresponding to a completely relaxed sample. Since the data recording of the rheometer and the optical setup was not synchronised in time, the time axis of respective data was shifted according to the point in time when shear was stopped. This might result in an offset between both data of up to 3 s. Furthermore, it has to be mentioned that the sample compositions slightly deviate from the samples investigated in Fig. 2, which might lead to quantitative differences in the obtained shear stress. Moreover, the shear protocols were adjusted to prevent the formation of artefacts such as bubbles or edge fracture of which even small amount of air passing the optical path would lead to a huge change in birefringence. Birefringence data was sampled with 1 Hz, whereas the first 10 s for sample A and B were sampled with 1 kHz.

The obtained birefringence together with the shear stress after cessation of flow is shown in Fig. S3 for all three systems, with the plot order following Fig. 2. For B and C the increase in shear stress is accompanied by an increase in birefringence, supporting that it is indeed an anisotropic distribution of local elastic inhomogeneities that impose stress on the polymer chains which is picked-up as an increase in birefringence. Furthermore, the qualitative similar evolution of birefringence and shear stress supports the choice of the shear stress as a measure for the anisotropic contribution of the reforming bonds in the second term on the right hand side of eq. 2.

Finally and importantly, for sample A we do not observe an intermediate stress upturn whereas the birefringence exhibits an intermediate plateau. However, these experiments were performed with the EHUT-dodecane solutions under humid conditions since our drying chamber developed for the rheometric tests could not fit the rheo-optical setup. Hence, we attribute the lack of stress upturn to the humidity which promotes chain scission as shown in Ref. [20]. This further supports the scenario put forth in this work, as the upturn requires the presence of large sections which will be further associated (see main text and Fig. 1).

### III. CESSATION OF FLOW UNDER DIFFERENT CONDITIONS AND ANALYSIS OF MOTOR DRIFT FOR SYSTEM A

In addition to the experiments performed with a strain controlled device, stress relaxation experiments were conducted with a stress controlled MCR 501 rheometer (Anton-Paar, Austria). Under those conditions, an increase in stress after cessation of flow could be observed as well (Fig. S4), indicating that the upturn in stress is independent of the utilized instrument.

The motor voltage output before imposing shear (when the motor is not moving), during the motor movement (transient), and after stopping the motor (during stress relaxation) is plotted in Fig. S5(a) for several shear rates applied to system A. The state of the motor voltage output before and after imposing the shear rate are identical, hence, indicating the absence of any uncontrolled motor movement during the relaxation process, which might cause the shear stress to increase. This becomes even more clear in Fig. S5(b) that presents the motor voltage just after flow is stopped. During the relaxation process, especially in the time window where the stress increases (0.2 s to 20 s in top graph of Fig. 2), no movement of the motor is detected.

---

[20] A. Louhichi, A. R. Jacob, L. Bouteiller, and D. Vlassopoulos, *J. Rheol.* **61**, 1173 (2017).

[21] M. Akbulut, N. K. Reddy, B. Bechtloff, S. Koltzenburg, J. Vermant, and R. K. Prud'homme, *Langmuir* **24**, 9636

(2008).

[22] G. G. Fuller, *Optical rheometry of complex fluids* (Oxford University Press on Demand, 1995).

[23] L. Pellens, J. Vermant, and J. Mewis, *Macromolecules* **38**, 1911 (2005).

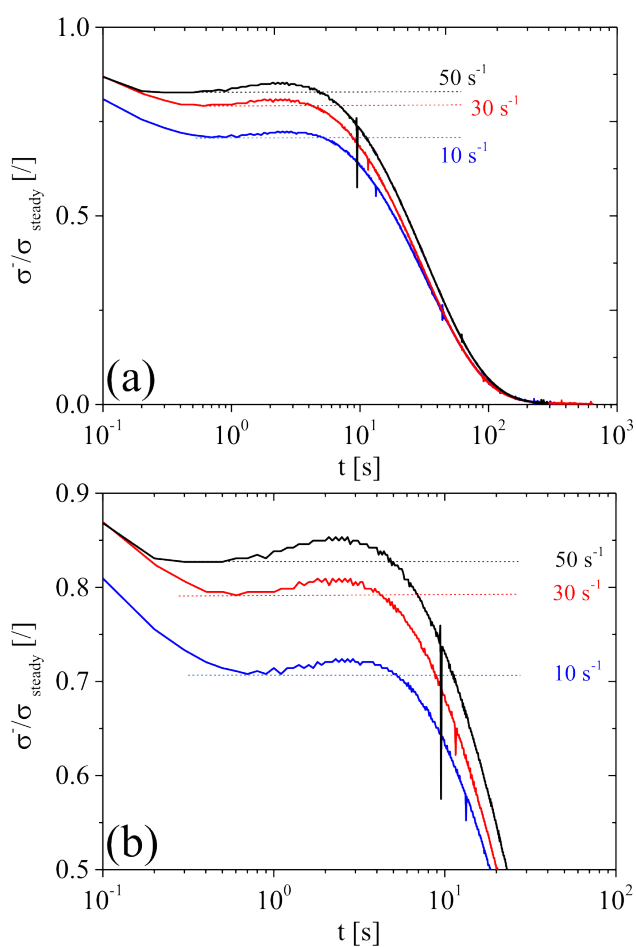


FIG. S4. a) Stress after cessation of flow  $\sigma^-$  normalized by the steady shear stress  $\sigma_{\text{steady}}$  as a function of time for system A, using a stress controlled rheometer. b) The same data as in (a) but magnified in order to highlight the stress upturn. Shear rates prior to cessation of flow are indicated in the figure.

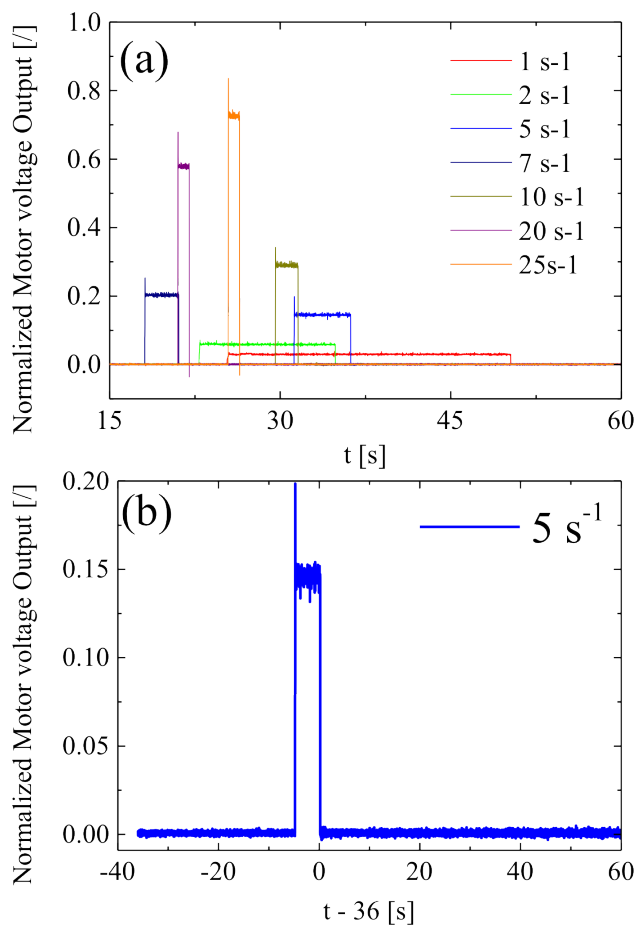


FIG. S5. a) The normalized (by 10 volts) motor voltage output measured by imposing different steady shear rates (as indicated in the figure) to the ARES strain controlled rheometer while recording the transient response of system A as presented in Fig. 2. b) The normalized motor voltage output measured during imposing a shear rate of  $5 \text{ s}^{-1}$  and by shifting the time axis with respect to the shear cessation.